inorganics

MDPI

Review

Redox-Active Manganese Pincers for Electrocatalytic CO_2 Reduction

Haley A. Petersen, Tessa H. T. Myren and Oana R. Luca *

Department of Chemistry, University of Colorado Boulder, 215 UCB Boulder, CO 80309-0215, USA; haley.petersen@colorado.edu (H.A.P.); tessa.myren@colorado.edu (T.H.T.M.)

* Correspondence: oana.luca@colorado.edu

Received: 17 October 2020; Accepted: 7 November 2020; Published: 11 November 2020

Abstract: The decrease of total amount of atmospheric CO_2 is an important societal challenge in which CO_2 reduction has an important role to play. Electrocatalytic CO_2 reduction with homogeneous catalysts is based on highly tunable catalyst design and exploits an abundant C_1 source to make valuable products such as fuels and fuel precursors. These methods can also take advantage of renewable electricity as a green reductant. Mn-based catalysts offer these benefits while incorporating a relatively cheap and abundant first-row transition metal. Historically, interest in this field started with Mn(bpy-R)$(CO)_3$X, whose performance matched that of its Re counterparts while achieving substantially lower overpotentials. This review examines an emerging class of homogeneous Mn-based electrocatalysts for CO_2 reduction, Mn complexes with meridional tridentate coordination also known as Mn pincers, most of which contain redox-active ligands that enable multi-electron catalysis. Although there are relatively few examples in the literature thus far, these catalysts bring forth new catalytic mechanisms not observed for the well-established Mn(bpy-R)$(CO)_3$X catalysts, and show promising reactivity for future studies.

Keywords: pincers; electrocatalysis; solar fuel; CO_2 upcycling; Mn(I); homogeneous catalysis

1. Introduction

CO_2 as a global challenge. Increased atmospheric levels of CO_2 pose a significant threat to our environment, while continued societal dependence upon fossil fuels leads to ever-increasing concentrations of this greenhouse gas [1–4]. Addressing these problems is critical to avoid increased ocean acidification and the potentially disastrous consequences of average planetary temperature increases, which include rising sea levels, increased desert formation, and widespread species extinction [5]. Current projections indicate that CO_2 emissions must reach net zero by 2070 to prevent exceeding the Paris Agreement benchmark of a 2 °C global temperature increase [4]. Furthermore, recent estimates based upon current emission trajectories place the likely average temperature increase for a doubling of atmospheric CO_2 somewhere between 2.3 °C and 4.5 °C, with decreasing likelihood of remaining below 2 °C [6].

Several CO_2-based methods of addressing this pressing problem exist, including the reduction of CO_2 emissions (decarbonization), the removal of CO_2 emissions through carbon capture and sequestration (CCS), and the recycling of emitted CO_2 into new products [5]. Decarbonization via the replacement of CO_2-emitting technologies with more environmentally benign alternatives will undoubtedly serve an important role in addressing climate change as key technologies such as wind and solar energy gradually replace their traditional fossil fuel-burning predecessors. However, these clean electricity technologies suffer from drawbacks such as intermittent production, meaning that their electrical outputs must be used immediately or lost in the absence of adequate storage technology [7]. Moreover, these technologies fail to address the persistent need for portable, combustible fuels in

sectors such as transportation. In contrast, CCS aims to pull emitted CO_2 either directly from emitting sources or from the atmosphere, trapping CO_2 emissions rather than preventing them. While this strategy could theoretically result in net negative CO_2 emissions, economic barriers often hinder large-scale implementation of carbon capture or necessitate its coupling to the further extraction of fossil fuels by using the captured CO_2 in enhanced oil recovery (EOR) [8]. This presents a clear obstacle in the face of long-term problems such as continued societal dependence upon fossil fuels.

The recycling of emitted CO_2 waste into value-added fuels or fuel precursors has the potential to address many of the above problems, creating a closed cycle from CO_2 emissions back to organic fuels while exploiting a potentially valuable and abundant C1 source. Closing this cycle using CO_2 as a chemical feedstock theoretically results in net-zero emissions and has the potential to financially incentivize the reduction of emissions, acting as a complement to carbon capture or decarbonization technologies. CO_2 reduction (CO_2R) can be coupled with carbon capture. Carbon capture and utilization (CCU) is a growing field predicted to use up to 700 million tons of CO_2 per year by 2050 [8,9], serving as a complement to CCS.

Electrocatalysis as an answer to the challenge. Although many CO_2R catalysts have been investigated, electrocatalytic CO_2 reduction in particular presents further benefits. Many chemical CO_2 reduction strategies have been explored but often require harsh conditions such as high temperature and pressure, high-energy reductants that are themselves energy-intensive to synthesize, or expensive precious metal catalysts, with relatively few reports of successful base metal-catalyzed reactions [10–13]. Electrocatalysis can operate under milder conditions while offering increased ability to interface with other emission mitigation strategies. Crucially, electrochemical methods are readily coupled to clean energy sources such as solar, enabling the production of solar fuels that effectively store intermittently generated energy for later use. This serves an important function in service of other renewable energy technologies while ensuring that the desired CO_2 reduction is carried out with electrons as a green reductant. While research on the production of other solar fuels such as hydrogen gas also shows promising developments [14], the reduction of CO_2 to liquid fuels, or precursors for such fuels, can exploit the existing infrastructure for liquid fossil fuels.

Electrocatalytic figures of merit. There are several figures of merit when comparing electrocatalysts, including overpotential, Faradaic efficiency (FE), selectivity, current density, and stability over time. FE is % measure of how much of the charge delivered to a system was used productively in the synthesis of product. Overpotential is an additional, distinct figure of merit that allows us to establish the necessary operating potential for a given catalyst to achieve a current density, usually defined at 10 mA cm^{-2}. Current density is a metric intrinsically related to overpotential. It is most often the maximal current obtained from a known surface area under a certain set of experimental conditions (i.e., a set potential) and is expressed in units of mA cm^{-2}, relying on estimations of electroactive surface area. Selectivity in the production of solar fuels is a key metric since protons and electrons, two of the ubiquitous reagents in such transformations, can combine to form hydrogen, rather than store hydrogen equivalents within the molecular framework of a storage molecule in the synthesis of a fuel. Faradaic efficiencies and selectivity are highlighted in this review, as they are the most common.

Molecular electrocatalysis for CO_2 reduction has been explored extensively due to high tunability through molecular design, often leading to improved selectivity over its heterogeneous counterpart [15,16]. Appropriately designed homogeneous catalysts also avoid the problems of electrode poisoning and the high overpotentials associated with obtaining sufficient current density in heterogeneous electrochemical CO_2 reduction [15–17]. Molecular catalysts based upon a variety of metals have been assessed for CO_2 reduction, particularly from group VII through group X [17]. Although several 4d and 5d metals such as Re [18–20], Ru [21–27], and Ir [28–31] have been investigated for CO_2 reduction with success, first-row transition metals are often preferred to their second- or third-row counterparts due to their higher earth abundance and lower cost. For this reason, established catalysts based upon the third-row group VII metal Re are frequently

substituted with analogues using Mn, the third most abundant transition metal in the Earth's crust [32]. Unlike group-based catalyst families using later transition metals, group VII catalysts frequently exhibit CO_2R activity regardless of whether the metal center is Mn or Re [17]. This offers valuable opportunities for comparison and insight.

Tridentate ligands that coordinate in a mer fashion, or pincers, have also resulted in a variety of complexes with demonstrated activity for CO_2 reduction [33]. Because of the potential for high selectivity and activity while maintaining lower costs, the present review focuses specifically on the current state of research on homogeneous electrocatalytic Mn pincer complexes for CO_2 reduction. This specific class of catalysts is of interest because they incorporate tridentate redox non-innocent ligands that can act as electron reservoirs, improve catalyst stability, and often result in mechanisms that diverge from more commonly reported bidentate bpy-based Mn systems.

2. Mn-Based Electrocatalysts in CO_2 Reduction

The first reported Mn-based CO_2R catalysts were *fac*-Mn(bpy-R)$(CO)_3$Br (bpy-R = 2,2′-bipyridine (bpy) (**1**) or 4,4′-dimethyl-2,2′-bipyridine (dmbpy (**2**), Figure 1) [34], structural analogues of a Re-based catalyst originally reported in 1984 [35]. Synthesis of **1** was initially reported in 1979 [36], but the complex was not studied for CO_2R catalysis until 2011 [34]. The *fac*-M(bpy-R)(CO_3)X catalysts therefore established promising structural motifs for CO_2R catalysis, inspiring many further reports that decorated the parent bpy ligand to modulate electronic or steric effects of the bidentate ligand, or substituted other X-type ligands for bromide [19,20,37–39]. A key element of these catalysts is the use of redox-active bpy ligands, enabling the storage of an additional e^- equivalent within the ligand framework. This surpasses the typical one-electron capacity common to abundant first-row transition metals in the +1 state. This enables multielectron catalysis by the complex [40], a necessary feature for CO_2R reactions that require a minimum of two electrons. This catalytic design is a strategy commonly employed in reaction development, conferring "nobility" to the first-row metals [40,41]. Catalysts of this class most often produce CO with high FE for the reaction shown in Equation (1),

$$CO_2 + 2H^+ + 2e^- \rightarrow CO + H_2O, \quad (1)$$

while other catalysts may exhibit products more consistent with reactions shown in Equations (2)–(4),

$$CO_2 + 2H^+ + 2e^- \rightarrow HCOOH, \quad (2)$$

$$CO_2 + 2H^+ + 2e^- \rightarrow H_2C_2O_4, \quad (3)$$

$$2CO_2 + 2e^- \rightarrow CO + CO_3^{2-} \quad (4)$$

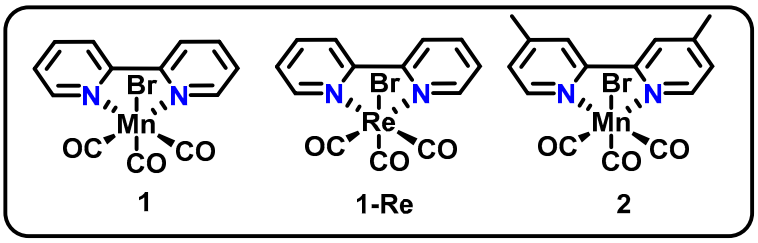

Figure 1. Structures of *fac*-Mn(bpy)$(CO)_3$Br (**1**) and *fac*-Mn(dmbpy)$(CO)_3$Br (**2**).

This established class of Mn-based electrocatalysts has been studied in depth, yielding mechanistic insights as depicted in Scheme 1. Entrance into the catalytic cycle is proposed to involve reduction by two electrons and X-ligand loss, after which CO_2 substrate may bind to the metal center and become protonated [42]. After this stage, the mechanism diverges into two possible paths, i.e., the reduction-first pathway (in red, proceeding through structure **f** in Scheme 1) or the protonation-first pathway (in blue,

proceeding through structure **e** in Scheme 1), the latter of which may occur at more positive potentials due to increased favorability of reducing a cationic species [17].

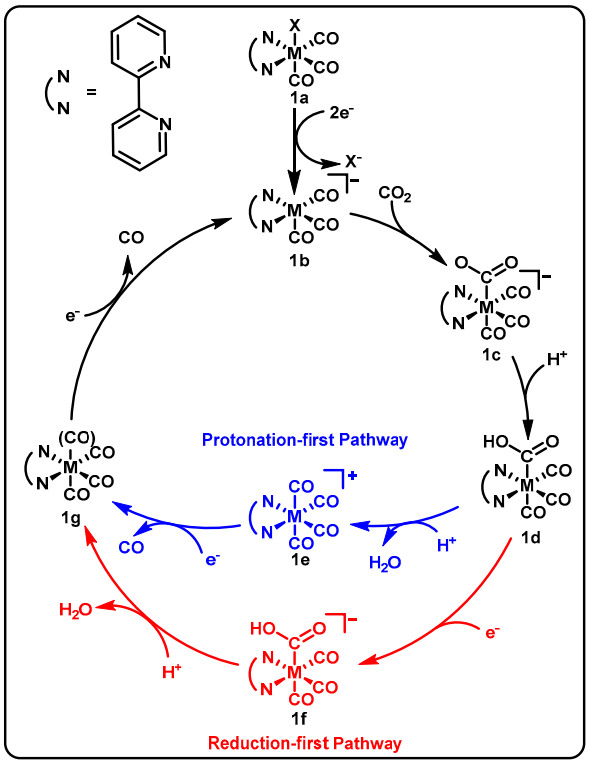

Scheme 1. Proposed mechanistic pathways of M(bpy)$(CO)_3$X structural Group 7 analogues of catalyst **1**, where M = Re (**1-Re)** or Mn (**1)** [42]. The protonation-first pathway is shown in blue, whereas the reduction-first pathway is shown in red.

Catalyst **2** (Figure 1) was found to operate at potentials 400 mV positive of its Re analogue in electrochemical experiments in 95/5 MeCN/H_2O and 0.1 M tetrabutylammonium perchlorate (TBAP) electrolyte, with comparable FE and selectivity. This is thought to be due to a sequence of steps upon entrance into the catalytic cycle (the conversion from **1a** to **1b** in Scheme 1) [42]. The Re catalyst **1-Re** requires the addition of a second equivalent of electrons prior to the dissociation of X^- due to the increased stability of the singly reduced $[Re(bpy)(CO)_3X]^{\bullet-}$ species, whereas the Mn version of the catalyst **1** more readily gives up X^- after only a single reduction to form either $[Mn(bpy)(CO)_3]^0$ or a dimerized form of the catalyst. This facilitates a second reduction at a more positive potential to yield **1b**. However, the Mn complex exhibits lower current densities and requires the use of a sacrificial proton source, unlike its Re counterpart **1-Re** [34,35], which was shown to most likely operate via the reduction-first pathway (Scheme 1, red). The reduction-first mechanistic pathway diverges from the protonation-first one by the acceptance of an additional reducing equivalent by **1d**, leading to the formation of **1f** instead of protonation leading to **1e**. The reduction step of the reduction-first pathway **1d→1f** is followed by a protonation/dehydration step to lead to the formation of **1g**, which in the case of Re retains all four carbonyl ligands. The Mn derivative is likely to lose one CO ligand to reach a 5-coordiante **1g** after the **1e→1g** step. The active catalyst **1b** is regenerated after an additional reduction, which in the case of **Re** occurs with loss of a CO ligand.

Nonetheless, installation of various substituents on the bpy ligand of the Mn-based catalyst have been shown to minimize overpotential by sterically preventing dimerization [38] or promoting the protonation-first pathway through use of hydrogen-bonding groups [39] (Scheme 1 blue), or to improve catalytic rate by increasing electron donation into the metal center [37].

With a promising background for Mn-based electrocatalysis established, the present review discusses budding research developments in Mn pincer complexes, an emerging class of Mn-based CO_2R electrocatalysts that illustrate novel reactivity motifs in the synthesis of solar fuels. Similarly to the $M(bpy)(CO)_3X$ catalysts, this class of complexes employs polydentate redox-active ligands for use as electron reservoirs that can enable multi-electron catalyses at metal centers that would normally be limited to one-electron-steps. Metals in the 1^+ oxidation state of group VII are examples of such species as they would normally be able to accept only one electron equivalent before reaching their M^0 state. While a simple 2,2′ bipyridine can act as an electron reservoir, the expansion of the ligand from a simple bidentate bpy derivative to a larger, conjugated tridentate pincer can additionally leverage the chelate effect to improve chemical and thermal stability of the complex and strength of the ligand-metal binding, provide additional opportunities to tune electron donation into the metal center, and enable novel mechanistic avenues for product formation [43].

3. Pincers in Mn CO_2 Reduction Electrocatalysts

Mn pincer complexes based upon a variety of ligand frameworks are discussed herein and organized by coordination type. Table 1 presents a summary of the key examples discussed below to allow for ease of comparison between them as well as the previously discussed benchmark $Mn(bpy\text{-}R)(CO)_3X$ catalysts. For each catalyst type, a brief discussion of analogous complexes based upon other metals centers is offered to examine the relationship between metal center identity and activity. The abbreviation of the pincer type is based on the elements in contact with the metal center-for example, **3b** is an ONN pincer with O, N and N being the elements of the pincer ligand that are attached to the metal.

Table 1. Summary of pincer catalysts discussed.

(Pre-)Catalyst	Pincer Type	Oxidation States	Products (FE, %)	Bulk Electrolysis Conditions	Proton Source	Ref.
3a (intermediate, Scheme 2)	ONN	Mn(I), Mn(0)	CO (70%), $HCOO^-$ (22%), H_2O	−1.8 V vs. SCE, 4 h, MeCN	none	[44]
			CO (90%), $HCOO^-$ (4%)	−1.5 V vs. SCE, 2 h, MeCN, 0.1M TBA PF_6	2.7 M H_2O	[45]
			CO (48%), $HCOO^-$ (36%)	−1.5 V vs. SCE, 2 h, MeCN, 0.1 M TBA PF_6	2.7 M TFE	
			CO (15%), $HCOO^-$ (39%)	−1.5 V vs. SCE, 2 h, MeCN, 0.1 M TBA PF_6	2.7 M phenol	
$Mn(\kappa^2\text{-tpy})(CO)_3Br$ (**4**, Figure 2)	NNN	Mn(I), Mn(0)	CO (129%) [1], H_2O	−2.2 V vs. Fc/Fc^+, MeCN, 0.1 M TBA PF_6, 4.1 turnovers	0.5 M phenol	[46,47]
$Mn(\kappa^3\text{-tpy})(CO)_2Br$ (**5**, Figure 2)	NNN	Mn(I), Mn(0)	CO (93%), H_2O	−2.2 V vs. Fc/Fc^+, MeCN, 0.1 M TBA PF_6, 4.1 turnovers	0.5 M phenol	
$MnPNP(CO)_3$ (**6**, Figure 3)	PNP	Mn(I), Mn(0)	CO (96%), CO_3^{2-}	−2.3 V vs. Fc/Fc^+, 125 min, MeCN, 0.1 M TBA PF_6	none	[48]
$MnCNC^{Me}$ (**7**, Figure 4)	CNC	Mn(I), Mn(0)	CO (87%), CO_3^{2-}	−2.3 V vs. Fc/Fc^+, MeCN, 0.1 M TBA PF_6	none	[49]
$MnCNC^{Bn}$ (**8**, Figure 4)	CNC	Mn(I), Mn(0)	CO (86%), CO_3^{2-} (93%)	−2.3 V vs. Fc/Fc^+, MeCN, 0.1 M TBA PF_6	none	[49,50]
$Mn(dmbpy)(CO)_3X$ (**2**, Figure 1)	-	Mn(I), Mn(0)	CO (100%), H_2O	138 C, −1.70 V vs. $Ag/AgNO_3$, 1mM cat in 95/5 MeCN/H_2O, 0.1 M TBAP	5% H_2O	[34]

[1] Loss of CO ligand from the pre-catalyst causes non-Faradaic CO production and increases this value above 100% [46,47].

3.1. ONN Pincer Binding in Mn(bpy-R)(CO)$_3$X Catalysts

Among the many examples of Mn(bpy-R)(CO)$_3$X catalysts reported, one example from 2014 (**3**, Scheme 2 and Table 1) that was initially believed to behave in a similar fashion to other catalysts of the class was later found to incorporate pincer intermediates [44,45]. Catalyst **3** was found to produce CO with 70% FE and formate/formic acid with 22% FE with the ligand as the sole proton source under an applied bias of −1.8 V vs. Fc/Fc$^+$. This performance, yielding a turnover frequency (TOF) of 1.4 s^{-1} and turnover number (TON) of 19 for CO production, compared favorably with the original Mn(bpy)(CO)$_3$Br catalyst. Cyclic voltammetry (CV) is an electrochemical technique that allows us to diagnose potentials necessary for the introduction of reducing equivalents into the molecular frameworks of catalysts. Such data showed that complex **3** underwent three reductions at −1.2 V vs. saturated calomel electrode (SCE), −1.51 V vs. SCE, and −1.66 V vs. SCE. Both the second and third reductive features showed gradual attenuation of current at higher scan rates, indicating the existence of a chemical step preceding each of the two reductions [44]. Although the chemical step preceding the second reduction was initially presumed to be dimerization (as expected for Mn(bpy-R)(CO)$_3$X catalysts), later studies using IR and UV/VIS spectroelectrochemistry (SEC) illustrate that this was not the case [45].

Scheme 2 presents the proposed pathway for catalyst activation for entrance into the catalytic cycle [45]. Although this example is based upon a bidentate pre-catalyst and bidentate active catalytic state, the ability of the phenoxide group to coordinate into the metal center is proposed to play a significant role in two intermediates, namely **3b** and **3c**, and may be responsible for the notable mechanistic differences between this catalyst and the canonical Mn(bpy-R)(CO)$_3$X catalysts. The ability of the ligand to become tridentate and donate an additional two electrons to the metal may provide an alternative route toward a stable 18-electron count for the complex, thus no longer favoring formation of a Mn–Mn bond.

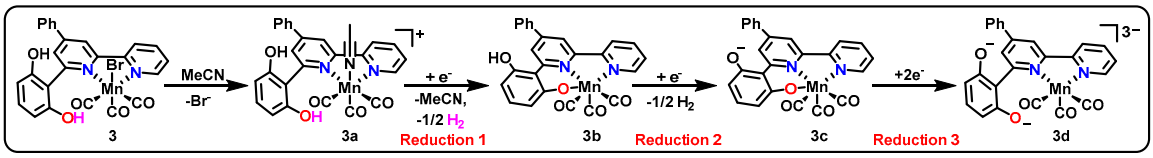

Scheme 2. Proposed mechanism of activation of **3** for entrance into a catalytic cycle for the production of CO and formate.

Additionally, the ligand itself can act as a proton source for catalysis, explaining the observation of formate production in the absence of added proton source [44]. In the presence of an external proton source, the products of catalysis for the complex were also found to be variable depending upon the proton source acidity [45]. While added water resulted in highly selective CO formation (90%), increasing acidity of the added proton source was found to increase the ratio of formate to CO. By changing the proton source from water to phenol, the CO and formate FE were changed from 90% and 4% to 15% and 39%, respectively, with the intermediate-acidity 3,3,3-trifluoroethanol (TFE) giving intermediate values of 48% and 36%, respectively. Efficiency for hydrogen production increases concomitantly with increasing efficiency for formate production, suggesting water as the best proton source for obtaining single-product selectivity as well as the highest overall efficiency.

Despite intriguing mechanistic insights and good FE for CO production under optimized conditions, **3** still lacks optimal catalyst stability. Bulk electrolysis of **3** shows an appreciable decrease in current, likely due to catalyst deactivation, within an hour of initiating electrolysis at −1.8 V vs. SCE in dry MeCN/tetrabutylammonium hexafluorophosphate (TBA PF_6) solution [44]. Furthermore, data for turnovers in excess of 28 for any given CO_2R product have not been reported for the catalyst [45]. While this work presents an interesting contrast to other Mn(bpy-R)-based systems, there is still further work to be done in examining routes to stable complexes that employ this framework.

3.2. NNN and tpy-Based Pincers

Another direct descendant of the Mn(bpy-R)$(CO)_3$X family is the Mn(tpy) pincer. Extending the classic bpy structure to contain a third binding site yields 2,2′:6′,2′′-terpyridine (tpy), which has been shown to be a good ligand for CO_2R catalysts of both Mn and Re. Building on an original report by Chardon-Noblat in 2014 [46], Machan and Kubiak studied CO_2R activity of two such catalysts in 2016, namely Mn(κ^2-tpy)$(CO)_3$Br (**4**) and Mn(κ^3-tpy)$(CO)_2$Br (**5**) (Figure 2) [47].

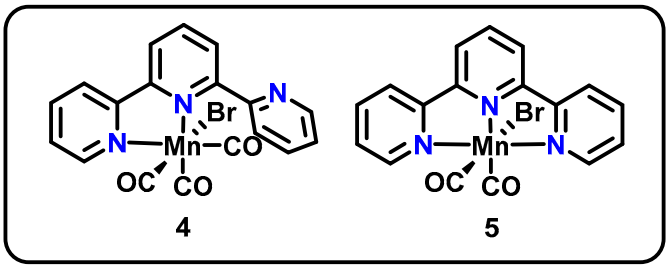

Figure 2. Structures of Mn(κ^2-tpy)$(CO)_3$Br (**4**) and Mn(κ^3-tpy)$(CO)_2$Br (**5**) [46,47].

Using CV, complex **4** shows reductive features at −1.56 V and −1.77 V vs. Fc/Fc^+ and irreversible oxidation features on the return sweep at −1.57 V and −0.99 V vs. Fc/Fc^+. Faster scan rates revealed an additional feature at −1.63 V vs. Fc/Fc^+. The CV response of **5** was remarkably similar, with irreversible reduction features at −1.56 V and −1.75 V and irreversible oxidation features at −1.57 V and −0.95 V vs. Fc/Fc^+. Fast scan rates again revealed an additional irreversible feature at −1.69 V vs. Fc/Fc^+. For each complex, the second irreversible reductions (−1.77 V for **4** and −1.75 V for **5**) and second irreversible oxidations (1–0.99 V; 2–0.95 V vs. Fc/Fc^+) were attributed to the reduction and oxidation (respectively) of a dimerized species (**4b**) presumably via **4a**, as shown in Scheme 3, using evidence from chemical reduction experiments and IR spectroelectrochemistry (SEC). From a scan rate analysis, the formation of this dimer was concluded to occur on a similar timescale to that of the CV experiment, a much slower timescale than that observed for catalysts with simple bidentate bpy ligands. Therefore, both **4** and **5** were found to access the same dimerized intermediate and active catalyst state **4c** as shown for **4** in Scheme 3. The authors conclude that the bidentate pre-catalyst **4** therefore can perform CO_2R using a κ^3 pincer-type coordination mode.

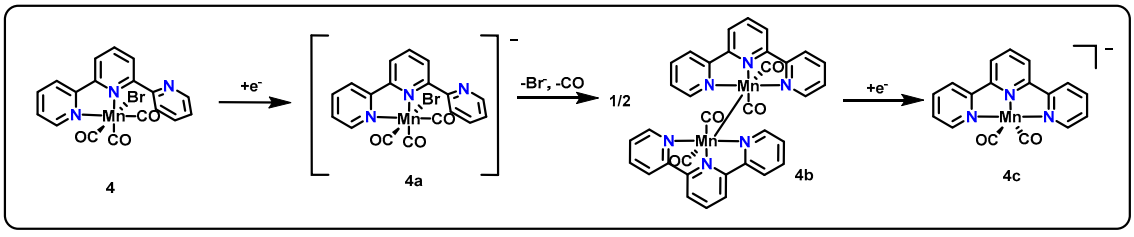

Scheme 3. Proposed mechanism for the reductive activation of **4**.

The dimerization, along with an observed first order in CO_2, suggest a large number of similarities between the mechanism of CO_2R for these complexes and that of the original Mn(bpy-R)$(CO)_3$X catalysts [47]. However, the notably slower dimerization of this system allows for competing pathways between dimer formation and CO_2 binding, enabling access to lower overpotentials. The success of the catalysts was further evidenced through 129% FE for CO for **4** (value exceeds 100% due to loss of a CO equivalent from pre-catalyst) and 93% FE for CO for **5**. However, these values were reflective of bulk electrolyses conducted through only the first 4.1 turnovers of the catalyst. Thereafter, catalyst degradation was observed, lowering overall FE and again pointing to stability issues with the catalyst.

In addition to group VII metals, terpy pincers of Ru have also been reported for CO_2R catalysis and have even been shown to produce C2 products when cooled to −20 °C [21,51]. Narayanan et al. also reported an additional NNN-type pincer complex of Ni for CO_2 reduction with aldimine binding rather than additional pyridyl side wings [52].

3.3. PNP Pincers

In a larger departure from the classical bpy-based catalysts, Rao et al. reported a CO_2R catalyst with an Mn center with PNP coordination to a pincer ligand (**6**, Figure 3) [48]. This catalyst produces both CO and carbonate, and interestingly is inhibited by H_2O addition, a clear contrast between this catalyst and its $Mn(bpy)(CO)_3Br$ predecessor. While few mechanistic insights were offered, the catalyst CVs reveal similar overpotential requirements to $Mn(bpy)(CO)_3Br$, with a catalytic onset of approximately −2.0 V vs. Fc/Fc^+. Similarly, the catalyst yielded excellent FE for CO in the absence of water (96% over 125 min). Despite unknowns, this system operates via a clearly different mechanism other than previous Mn-based CO_2R examples. Catalyst **6** highlights the potentially significant contributions of pincer frameworks to the field in discovering alternate routes to CO_2 reduction.

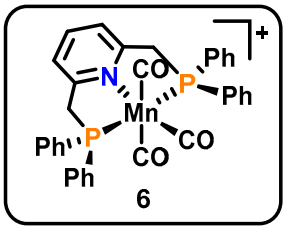

Figure 3. Structure of the PNP Mn pincer catalyst **6** [48].

A wide variety of other CO_2R catalysts containing PNP pincer frameworks have been reported with a large range of metal centers and ligands [28,31,33], including the only known successful Rh CO_2R electrocatalyst [53].

3.4. CNC Pincers

Pincers incorporating metal–carbon bonds from N-heterocyclic carbenes (NHCs) have generated interest due to the strong sigma donation available from NHCs, opening the possibility for increased electron density on the metal center and thus increased reactivity for CO_2 reduction. In 2018, the following two CNC manganese catalysts using NHC frameworks to promote CO_2R were reported: **7** $[MnCNC^{Me}(CO)_3]Br$ and **8** $[MnCNC^{Bn}(CO)_3]Br$ (Figure 4) [49]. The activity of these catalysts diverges substantially from the proposed mechanisms of the benchmark $Mn(bpy\text{-}R)(CO)_3X$, resulting in protonless operation and production of carbonate, CO_3^{2-} [50], as shown in Scheme 4. The molecular structure of **7** from X-ray crystallography indicated the expected octahedral coordination and outer-sphere bromide. A geometric distortion of the pyridine ring was also observed, suggesting a delocalized molecular orbital and the ligand acting as an electron reservoir.

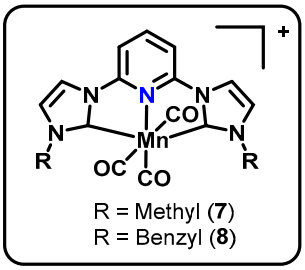

Figure 4. Structures of complexes **7** ($[MnCNC^{Me}(CO)_3]Br$) and **8** ($[MnCNC^{Bn}(CO)_3]Br$).

CV experiments demonstrated activity under an atmosphere of CO_2 both with and without a proton source present. Current densities up to 16 mA/cm^2 are obtained in the absence of protons. Compared to activity under inert atmosphere, **8** [MnCNC^{Me}(CO)$_3$]Br and **7** [MnCNC^{Bn}(CO)$_3$]Br displayed 18- and 21-fold current increases under CO_2, respectively. Turnover was shown to occur with 1e$^-$ per manganese center, based on results from the combined techniques of diffusion ordered spectroscopy (DOSY) and normal pulse voltammetry (NPV) as described by Donadt et al. [54].

Initial controlled potential electrolysis experiments at −2.3 V vs. Fc/Fc$^+$ determined an FE of 87% ± 3% and 86% ± 4%, respectively, for the methyl- and benzyl-substituted complexes and further product analysis by derivatization and GC–MS–EI found carbonate to be the second product of the protonless reaction with the above 95% current efficiencies. Further CV experiments determined a second order in CO_2 by using the resulting currents from varying CO_2 concentrations as relative rates and a half-order in catalyst by varying catalyst concentration. The latter determination was the first example of the Burés normalized timescale method [50] being used to determine the order in catalyst from voltammetry data. The proposed mechanism (Scheme 4) begins with the reduction of two equivalents of the metal complex **7** followed by the loss of two CO each to form a square planar Mn^0 species **7a**. One equivalent of CO_2 is then bound between two manganese centers to form **7b** before a second CO_2 inserts into the complex to arrive at **7c**. A final rearrangement produces a bimetallic carbonate complex **7d**, which then releases the carbonate and regenerates the square planar Mn^0 species **7a**.

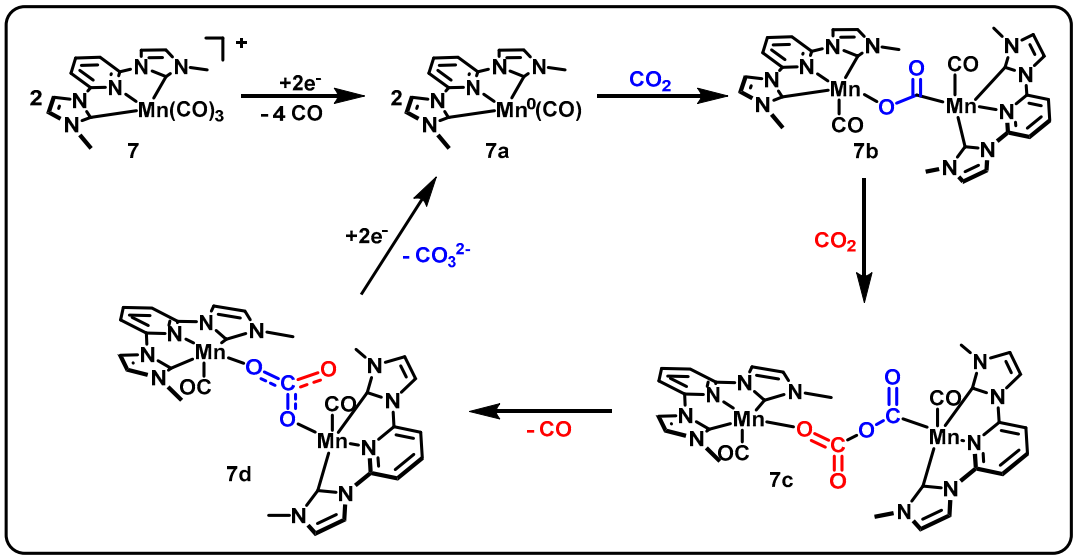

Scheme 4. Proposed mechanism of [MnCNC^{Me}(CO)$_3$]Br, adapted from [50] with permission.

Other CNC ligand frameworks have been investigated for CO_2 reduction. A Re analogue, [ReCNC^{Bn}(CO)$_3$]Cl, was synthesized and investigated but, unlike other Re analogues, showed little catalytic response to CO_2 [55]. This behavior is unlike previous studied group VII catalysts, as discussed above. Density Functional Theory (DFT) calculations showed that between the reduced forms (**7a** for Mn) of the two complexes, the Mn complex demonstrates increased metalloradical character (66%) while the Re has a much lower radical character on the metal (38%), suggesting that the reduced Re complex may not be sufficiently nucleophilic for CO_2 reduction [50]. A second explanation for this observation would be that the CO ligands are too strongly bound to allow coordination of a new CO_2 ligand. Calculations also showed that the Mn complex has unique access to a square planar intermediate with a single bound CO that is not accessible to the Re complex, possibly due to differences in orbital populations upon reduction.

Group X metals, however, have shown some precedence for successful CO_2R by CNC pincer complexes having square planar or pseudo-square planar geometries [33,56–58]. While many early examples based on Pd exhibit low efficiencies for CO_2 reduction, instead favoring hydrogen evolution [56–58], progress has been made with current PdCNC pincer complexes exceeding FE of 50% for CO [59].

4. Conclusions

The use of pincer-type ligands for Mn-based CO_2R electrocatalysts presents a promising future direction for CO_2R catalysis. Current vignettes of CO_2R have been reported with CNC, NNN, and PNP ligand frameworks, along with an interesting report of ONN intermediate pincer binding. These complexes incorporate the relatively abundant and low-cost Mn in place of expensive and rare noble metals while frequently exhibiting high catalytic rates and good selectivity for CO_2R under optimized conditions. The use of pincer-type ligands enables novel mechanistic pathways that diverge from those of the oft-discussed $Mn(bpy)(CO)_3X$ catalysts whose performance serves as a benchmark for other Mn-based catalysts.

Despite these advances and promising preliminary results, there is still much work to be performed to achieve improved overpotentials and catalyst stability. Many of the catalysts discussed herein are sensitive to water or oxygen or do not have extensive data reported regarding their long-term stability. While FE for the reported bulk electrolysis experiments shows excellent CO_2 conversion, these values are indicative of short timescales on the order of single hours and catalyst turnovers lying only in the double digits. Future work will likely focus on identifying the limits of catalyst stability and improve this metric to make the catalysts more industrially relevant.

Funding: The authors would like to thank the University of Colorado for the generous funding of this research.

Acknowledgments: T.M. would like to thank the Department of Chemistry at CU Boulder for the Sewall Fellowship.

Conflicts of Interest: The authors declare no conflict of interest.

References

1. IPCC. *Climate Change 2014: Synthesis Report*; Intergovernmental Panel on Climate Change: Geneva, Switzerland, 2014.
2. Cox, P.M.; Betts, R.A.; Jones, C.D.; Spall, S.A.; Totterdell, I.J. Acceleration of global warming due to carbon-cycle feedbacks in a coupled climate model. *Nature* **2000**, *408*, 184–187. [CrossRef]
3. Solomon, S.; Plattner, G.-K.; Knutti, R.; Friedlingstein, P. Irreversible climate change due to carbon dioxide emissions. *Proc. Natl. Acad. Sci. USA* **2009**, *106*, 1704–1709. [CrossRef] [PubMed]
4. IPCC. *Global Warming of 1.5 °C*; WHO: Geneva, Switzerland, 2018.
5. Mikkelsen, M.; Jørgensen, M.; Krebs, F.C. The teraton challenge. A review of fixation and transformation of carbon dioxide. *Energy Environ. Sci.* **2010**, *3*, 43–81. [CrossRef]
6. Sherwood, S.; Webb, M.J.; Annan, J.D.; Armour, K.C.; Forster, P.M.; Hargreaves, J.C.; Hegerl, G.; Klein, S.A.; Marvel, K.D.; Rohling, E.J.; et al. An assessment of Earth's climate sensitivity using multiple lines of evidence. *Rev. Geophys.* **2020**, *58*, e2019RG000678. [CrossRef] [PubMed]
7. Whittingham, M.S. History, Evolution, and Future Status of Energy Storage. *Proc. IEEE* **2012**, *100*, 1518–1534. [CrossRef]
8. Global CCS Institute. *The Global Status of CCS: 2019*; Global Carbon Capture and Storage Institute Ltd: Melbourne, Australia, 2019.
9. Mac Dowell, N.; Fennell, P.S.; Shah, N.; Maitland, G.C. The role of CO_2 capture and utilization in mitigating climate change. *Nat. Clim. Chang.* **2017**, *7*, 243–249. [CrossRef]
10. Kar, S.; Goeppert, A.; Kothandaraman, J.; Prakash, G.K.S. Manganese-Catalyzed Sequential Hydrogenation of CO_2 to Methanol via Formamide. *ACS Catal.* **2017**, *7*, 6347–6351. [CrossRef]
11. Schneidewind, J.; Adam, R.; Baumann, W.; Jackstell, R.; Beller, M. Low-Temperature Hydrogenation of Carbon Dioxide to Methanol with a Homogeneous Cobalt Catalyst. *Angew. Chem. Int. Ed.* **2017**, *56*, 1890–1893. [CrossRef]

12. Behrens, M.; Studt, F.; Kasatkin, I.; Kuhl, S.; Havecker, M.; Abild-Pedersen, F.; Zander, S.; Girgsdies, F.; Kurr, P.; Kniep, B.L.; et al. The Active Site of Methanol Synthesis over $Cu/ZnO/Al_2O_3$ Industrial Catalysts. *Science* **2012**, *336*, 893–897. [CrossRef]
13. Yang, X.; Chen, X. Chapter 5—Mechanistic Insights and Computational Prediction of Base Metal Pincer Complexes for Catalytic Hydrogenation and Dehydrogenation Reactions. In *Pincer Compounds*; Morales-Morales, D., Ed.; Elsevier: Amsterdam, The Netherlands, 2018; pp. 101–110.
14. Gao, S.; Fan, W.; Liu, Y.; Jiang, D.; Duan, Q. Artificial water-soluble systems inspired by [FeFe]-hydrogenases for electro- and photocatalytic hydrogen production. *Int. J. Hydrog. Energy* **2020**, *45*, 4305–4327. [CrossRef]
15. Peterson, A.A.; Nørskov, J.K. Activity Descriptors for CO_2 Electroreduction to Methane on Transition-Metal Catalysts. *J. Phys. Chem. Lett.* **2012**, *3*, 251–258. [CrossRef]
16. Nam, D.-H.; De Luna, P.; Rosas-Hernández, A.; Thevenon, A.; Li, F.; Agapie, T.; Peters, J.C.; Shekhah, O.; Eddaoudi, M.; Sargent, E.H. Molecular enhancement of heterogeneous CO_2 reduction. *Nat. Mater.* **2020**, *19*, 266–276. [PubMed]
17. Jiang, C.; Nichols, A.W.; Machan, C.W. A look at periodic trends in d-block molecular electrocatalysts for CO_2 reduction. *Dalton Trans.* **2019**, *48*, 9454–9468. [CrossRef] [PubMed]
18. Smieja, J.M.; Kubiak, C.P. Re(bipy-tBu) $(CO)_3Cl$−improved Catalytic Activity for Reduction of Carbon Dioxide: IR-Spectroelectrochemical and Mechanistic Studies. *Inorg. Chem.* **2010**, *49*, 9283–9289. [CrossRef]
19. Sung, S.; Kumar, D.; Gil-Sepulcre, M.; Nippe, M. Electrocatalytic CO_2 Reduction by Imidazolium-Functionalized Molecular Catalysts. *J. Am. Chem. Soc.* **2017**, *139*, 13993–13996. [CrossRef]
20. Clark, M.L.; Cheung, P.L.; Lessio, M.; Carter, E.A.; Kubiak, C.P. Kinetic and Mechanistic Effects of Bipyridine (bpy) Substituent, Labile Ligand, and Brønsted Acid on Electrocatalytic CO_2 Reduction by Re(bpy) Complexes. *ACS Catal.* **2018**, *8*, 2021–2029. [CrossRef]
21. Chen, Z.; Chen, C.; Weinberg, D.R.; Kang, P.; Concepcion, J.J.; Harrison, D.P.; Brookhart, M.S.; Meyer, T.J. Electrocatalytic reduction of CO_2 to CO by polypyridyl ruthenium complexes. *Chem. Commun.* **2011**, *47*, 12607–12609. [CrossRef]
22. Machan, C.W.; Sampson, M.D.; Kubiak, C.P. A Molecular Ruthenium Electrocatalyst for the Reduction of Carbon Dioxide to CO and Formate. *J. Am. Chem. Soc.* **2015**, *137*, 8564–8571. [CrossRef]
23. Johnson, B.A.; Maji, S.; Agarwala, H.; White, T.A.; Mijangos, E.; Ott, S. Activating a Low Overpotential CO_2 Reduction Mechanism by a Strategic Ligand Modification on a Ruthenium Polypyridyl Catalyst. *Angew. Chem. Int. Ed. Engl.* **2016**, *55*, 1825–1829. [CrossRef]
24. Chen, Z.; Kang, P.; Zhang, M.-T.; Meyer, T.J. Making syngas electrocatalytically using a polypyridyl ruthenium catalyst. *Chem. Commun.* **2014**, *50*, 335–337. [CrossRef]
25. Chen, Z.; Concepcion, J.J.; Brennaman, M.K.; Kang, P.; Norris, M.R.; Hoertz, P.G.; Meyer, T.J. Splitting CO_2 into CO and O_2 by a single catalyst. *Proc. Natl. Acad. Sci. USA* **2012**, *109*, 15606–15611. [CrossRef] [PubMed]
26. Daryanavard, M.; Hadadzadeh, H.; Weil, M.; Farrokhpour, H. Electrocatalytic reduction of CO_2 to CO in the presence of a mononuclear polypyridyl ruthenium(II) complex. *J. CO_2 Util.* **2017**, *17*, 80–89. [CrossRef]
27. Lilio, A.M. *Bi-Functional Molecular Catalysts for CO_2 Reduction*; UC San Diego: San Diego, CA, USA, 2015.
28. Hu, G.; Jiang, J.J.; Kelly, H.R.; Matula, A.J.; Wu, Y.; Romano, N.; Mercado, B.Q.; Wang, H.; Batista, V.S.; Crabtree, R.H.; et al. Surprisingly big linker-dependence of activity and selectivity in CO_2 reduction by an iridium(I) pincer complex. *Chem. Commun.* **2020**, *56*, 9126–9129. [CrossRef] [PubMed]
29. Kang, P.; Cheng, C.; Chen, Z.; Schauer, C.K.; Meyer, T.J.; Brookhart, M. Selective Electrocatalytic Reduction of CO_2 to Formate by Water-Stable Iridium Dihydride Pincer Complexes. *J. Am. Chem. Soc.* **2012**, *134*, 5500–5503. [CrossRef] [PubMed]
30. Cao, L.; Sun, C.; Sun, N.; Meng, L.; Chen, D. Theoretical mechanism studies on the electrocatalytic reduction of CO_2 to formate by water-stable iridium dihydride pincer complex. *Dalton Trans.* **2013**, *42*, 5755. [CrossRef] [PubMed]
31. Feller, M.; Gellrich, U.; Anaby, A.; Diskin-Posner, Y.; Milstein, D. Reductive Cleavage of CO_2 by Metal–Ligand-Cooperation Mediated by an Iridium Pincer Complex. *J. Am. Chem. Soc.* **2016**, *138*, 6445–6454. [CrossRef] [PubMed]
32. Weast, R.C. *CRC Handbook of Chemistry and Physics*; CRC Press: Boca Raton, FL, USA, 1988.
33. Eberhardt, N.A.; Guan, H. *Reduction of CO_2 Mediated or Catalyzed by Pincer Complexes*; Elsevier: Amsterdam, The Netherlands, 2018; pp. 67–99.

34. Bourrez, M.; Molton, F.; Chardon-Noblat, S.; Deronzier, A. [Mn(bipyridyl)$(CO)_3$Br]: An Abundant Metal Carbonyl Complex as Efficient Electrocatalyst for CO_2 Reduction. *Angew. Chem. Int. Ed.* **2011**, *50*, 9903–9906. [CrossRef]
35. Hawecker, J.; Lehn, J.-M.; Ziessel, R. Electrocatalytic reduction of carbon dioxide mediated by Re(bipy)$(CO)_3$Cl (bipy = 2,2′-bipyridine). *J. Chem. Soc. Chem. Commun.* **1984**, 328–330. [CrossRef]
36. Staal, L.H.; Oskam, A.; Vrieze, K. The syntheses and coordination properties of M$(CO)_3$X(DAB) (M = Mn, Re; X = Cl, Br, I.; DAB = 1,4-diazabutadiene). *J. Organomet. Chem.* **1979**, *170*, 235–245. [CrossRef]
37. Smieja, J.M.; Sampson, M.D.; Grice, K.A.; Benson, E.E.; Froehlich, J.D.; Kubiak, C.P. Manganese as a Substitute for Rhenium in CO_2 Reduction Catalysts: The Importance of Acids. *Inorg. Chem.* **2013**, *52*, 2484–2491. [CrossRef]
38. Sampson, M.D.; Kubiak, C.P. Manganese Electrocatalysts with Bulky Bipyridine Ligands: Utilizing Lewis Acids to Promote Carbon Dioxide Reduction at Low Overpotentials. *J. Am. Chem. Soc.* **2016**, *138*, 1386–1393. [CrossRef]
39. Ngo, K.T.; McKinnon, M.; Mahanti, B.; Narayanan, R.; Grills, D.C.; Ertem, M.Z.; Rochford, J. Turning on the Protonation-First Pathway for Electrocatalytic CO_2 Reduction by Manganese Bipyridyl Tricarbonyl Complexes. *J. Am. Chem. Soc.* **2017**, *139*, 2604–2618. [CrossRef]
40. Luca, O.R.; Crabtree, R.H. Redox-active ligands in catalysis. *Chem. Soc. Rev.* **2013**, *42*, 1440–1459. [CrossRef]
41. Chirik, P.J.; Wieghardt, K. Radical Ligands Confer Nobility on Base-Metal Catalysts. *Science* **2010**, *327*, 794–795. [CrossRef] [PubMed]
42. Riplinger, C.; Sampson, M.D.; Ritzmann, A.M.; Kubiak, C.P.; Carter, E.A. Mechanistic Contrasts between Manganese and Rhenium Bipyridine Electrocatalysts for the Reduction of Carbon Dioxide. *J. Am. Chem. Soc.* **2014**, *136*, 16285–16298. [CrossRef] [PubMed]
43. Lawrence, M.A.W.; Green, K.-A.; Nelson, P.N.; Lorraine, S.C. Review: Pincer ligands—Tunable, versatile and applicable. *Polyhedron* **2018**, *143*, 11–27. [CrossRef]
44. Franco, F.; Cometto, C.; Ferrero Vallana, F.; Sordello, F.; Priola, E.; Minero, C.; Nervi, C.; Gobetto, R. A local proton source in a [Mn(bpy-R)$(CO)_3$Br]-type redox catalyst enables CO_2 reduction even in the absence of Brønsted acids. *Chem. Commun.* **2014**, *50*, 14670–14673. [CrossRef] [PubMed]
45. Franco, F.; Cometto, C.; Nencini, L.; Barolo, C.; Sordello, F.; Minero, C.; Fiedler, J.; Robert, M.; Gobetto, R.; Nervi, C. Local Proton Source in Electrocatalytic CO_2 Reduction with [Mn(bpy-R)$(CO)_3$Br] Complexes. *Chem. A Eur. J.* **2017**, *23*, 4782–4793. [CrossRef]
46. Compain, J.-D.; Bourrez, M.; Haukka, M.; Deronzier, A.; Chardon-Noblat, S. Manganese carbonyl terpyridyl complexes: Their synthesis, characterization and potential application as CO-release molecules. *Chem. Commun.* **2014**, *50*, 2539–2542. [CrossRef]
47. Machan, C.W.; Kubiak, C.P. Electrocatalytic reduction of carbon dioxide with Mn(terpyridine) carbonyl complexes. *Dalton Trans.* **2016**, *45*, 17179–17186. [CrossRef]
48. Rao, G.K.; Pell, W.; Korobkov, I.; Richeson, D. Electrocatalytic reduction of CO_2 using Mn complexes with unconventional coordination environments. *Chem. Commun.* **2016**, *52*, 8010–8013. [CrossRef] [PubMed]
49. Myren, T.H.T.; Lilio, A.M.; Huntzinger, C.G.; Horstman, J.W.; Stinson, T.A.; Donadt, T.B.; Moore, C.; Lama, B.; Funke, H.H.; Luca, O.R. Manganese N-Heterocyclic Carbene Pincers for the Electrocatalytic Reduction of Carbon Dioxide. *Organometallics* **2019**, *38*, 1248–1253. [CrossRef]
50. Myren, T.H.T.; Alherz, A.; Thurston, J.R.; Stinson, T.A.; Huntzinger, C.G.; Musgrave, C.B.; Luca, O.R. Mn-Based Molecular Catalysts for the Electrocatalytic Disproportionation of CO_2 into CO and CO_3^{2-}. *ACS Catal.* **2020**, *10*, 1961–1968. [CrossRef]
51. Nagao, H.; Mizukawa, T.; Tanaka, K. Carbon-Carbon Bond Formation in the Electrochemical Reduction of Carbon Dioxide Catalyzed by a Ruthenium Complex. *Inorg. Chem.* **1994**, *33*, 3415–3420. [CrossRef]
52. Narayanan, R.; McKinnon, M.; Reed, B.R.; Ngo, K.T.; Groysman, S.; Rochford, J. Ambiguous electrocatalytic CO_2 reduction behaviour of a nickel bis(aldimino)pyridine pincer complex. *Dalton Trans.* **2016**, *45*, 15285–15289. [CrossRef]
53. Vogt, M.; Nerush, A.; Diskin-Posner, Y.; Ben-David, Y.; Milstein, D. Reversible CO_2 binding triggered by metal–ligand cooperation in a rhenium(I) PNP pincer-type complex and the reaction with dihydrogen. *Chem. Sci.* **2014**, *5*, 2043–2051. [CrossRef]

54. Donadt, T.B.; Lilio, A.M.; Stinson, T.A.; Lama, B.; Luca, O.R. DOSY NMR and Normal Pulse Voltammetry for the Expeditious Determination of Number of Electrons Exchanged in Redox Events. *Chem. Sel.* **2018**, *3*, 7410–7415. [CrossRef]
55. Myren, T.H.T.; Alherz, A.; Stinson, T.A.; Huntzinger, C.G.; Lama, B.; Musgrave, C.; Luca, O.R. Metalloradical intermediates in electrocatalytic reduction of CO_2 to CO: Mn versus Re bis-N-heterocyclic carbene pincers. *Dalton Trans.* **2020**, *49*, 2053–2057. [CrossRef]
56. Therrien, J.A.; Wolf, M.O. The Influence of para Substituents in Bis(N-Heterocyclic Carbene) Palladium Pincer Complexes for Electrocatalytic CO_2 Reduction. *Inorg. Chem.* **2017**, *56*, 1161–1172. [CrossRef]
57. Therrien, J.A.; Wolf, M.O.; Patrick, B.O. Polyannulated Bis(N-heterocyclic carbene)palladium Pincer Complexes for Electrocatalytic CO_2 Reduction. *Inorg. Chem.* **2015**, *54*, 11721–11732. [CrossRef]
58. Therrien, J.A.; Wolf, M.O.; Patrick, B.O. Electrocatalytic Reduction of CO_2 with Palladium Bis-N-heterocyclic Carbene Pincer Complexes. *Inorg. Chem.* **2014**, *53*, 12962–12972. [CrossRef] [PubMed]
59. Therrien, J.A.; Wolf, M.O.; Patrick, B.O. Synthesis and comparison of nickel, palladium, and platinum bis(N-heterocyclic carbene) pincer complexes for electrocatalytic CO_2 reduction. *Dalton Trans.* **2018**, *47*, 1827–1840. [CrossRef] [PubMed]